DETC2017-67381

PARAMETRIC EXCITATION OF A REPULSIVE FORCE ACTUATOR

Mark Pallay Shahrzad Towfighian*

Department of Mechanical Engineering Binghamton University Binghamton, New York, 13902 mpallay1@binghamton.edu stowfigh@binghamton.edu

ABSTRACT

Parametric resonances in a repulsive-force MEMS resonator are investigated. The repulsive force is generated through electrostatic fringe fields that arise from a specific electrode configuration. Because of the nature of the electrostatic force, parametric resonance occurs in this system and is predicted using Mathieu's Equation. Governing equations of motion are solved using numerical shooting techniques and show both parametric and subharmonic resonance at twice the natural frequency. The primary instability tongue for parametric resonance is also mapped. This is of particular interest for MEMS sensors that require high signal-to-noise ratios due to the large oscillation amplitudes associated with parametric resonance.

INTRODUCTION

Microelectromechanical systems (MEMS) are highly integrated in many high-tech electrical devices such a smartphones, transducers, digital displays, stability control systems, hearing aids, and many more. Many resonators that require actuation utilize electrostatic forces due to the fast response time, low power consumption, and ease of fabrication/implementation [1]. This comes with the trade off of being highly nonlinear and susceptible to the pull-in phenomena, where electrostatic forces between two electrodes become so large that they collapse together. Be-

Traditional electrostatic actuation involves attractive forces between two electrodes with a voltage potential between them. Some effort has been put into developing electrostatic actuation where two electrodes are pushed away from each other as a way of eliminating pull-in and increasing stroke [2-11]. In 2001, Lee and Cho [2] studied an electrode configuration that results in two grounded electrodes being repelled from each other. If a charged electrode is placed along the side of two grounded electrodes (one fixed, one movable), the movable electrode moves in the opposite direction of the fixed electrode. He and Ben-Mrad used this same principle to create out-of-plane actuation [5] by flipping Lee's design on its side. In this configuration, the actuator is suspended above three electrodes (shown in Fig.1). The two side electrodes are charged while the beam and center electrode are grounded. This was shown to achieve large out-of-plane actuation, however it requires a high voltage potential due to the weak forcing associated with fringe electrostatic fields. However, the scope of their study was limited to static applications.

The authors have recently extended the study from He and Ben-Mrad to include dynamic applications [12]. We conducted dynamic experiments, superimposing an AC component to the DC voltage on the side electrodes, finding softening nonlinear-

cause these drawbacks limit the performance of MEMS devices (and therefore the performance of the devices that use them), improvements to electrostatic MEMS that address these issues are very valuable.

^{*}Address all correspondence to this author.

ities associated with the repulsive force. Because of the nature of the repulsive force (from the electrode configuration shown in Fig.1), the system should also show parametric resonance, which can be used for improving sensitivity of many sensors.

Parametric excitation (PE) has been applied to MEMS devices since 1990 [13] and since then has been used in many resonator designs [14–18]. PE involves exciting a system using time-varying parameters of the system, rather than direct forcing. This can be achieved by placing two electrodes along the length of the resonator [19] where the beam is simultaneously pulled towards both electrodes. These designs are still susceptible to pull-in, which limits the response amplitude. In 2013, Linzon et al [20] designed a fringe field parametric resonator that eliminates the pull-in instability and can theoretically attain large oscillation amplitudes. However, this design requires an initial displacement or a curved micro-beam to operate because there is no net force on the resonator when the beam is at its rest position.

In this paper, parametric resonance of the actuator proposed in [5] is studied. The layout of the beam/electrodes is shown in Fig.1 and the beam is assumed to have cantilever boundary conditions. Unlike other parametric resonators, this design pushes the beam away from the electrodes, which eliminates pull-in and allows large oscillation amplitudes. It also generates a net force on the beam in its rest position so no initial displacement is necessary for its operation, which can be utilize both normal and parametric resonances. When a voltage is applied to the side electrodes, the electrostatic forces generate a positive stiffening effect on the cantilever, as confirmed in our previous experiment [12]. By changing the voltage on the side electrodes, the effective stiffness of the micro-structure can be changed. By modulating this at twice the natural frequency (with electrostatic stiffening effects), the system should show parametric resonance. The motivation of this work is to study parametric resonance of this electrode configuration for sensors where a large signal-tonoise ratio is required.

The organization of this paper is as follows: In the next section, the formulation of the governing equation of motion is outlined. Next, the relation to Mathieu's Equation is defined and the location of primary parametric resonance is estimated. Then the theoretical results from the model are presented. Lastly, our conclusions based on the simulation results are given.

THEORETICAL MODEL Formulation

The beam is assumed to be linear-elastic polysilicon with dimensions given in Tab. 1. Axial displacement and beam stretching are ignored. The governing equation is obtained using Euler-Bernoulli beam theory and is given as,

$$\rho A \frac{\partial^2 \hat{w}}{\partial \hat{t}^2} + \hat{c} \frac{\partial \hat{w}}{\partial \hat{t}} + EI \frac{\partial^4 \hat{w}}{\partial \hat{x}^4} + \hat{f}_e(\hat{w}) V^2 = 0$$
 (1)

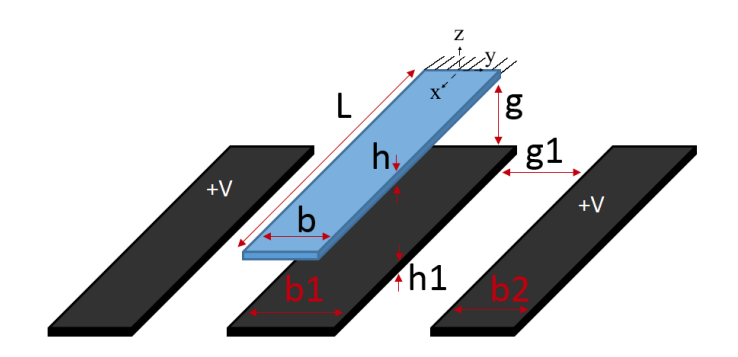


FIGURE 1. ELECTRODE CONFIGURATION OF THE RESONATOR AS DESIGNED IN [5]. CANTILEVER IS SHOWN IN BLUE AND THE ELECTRODES ARE BLACK.

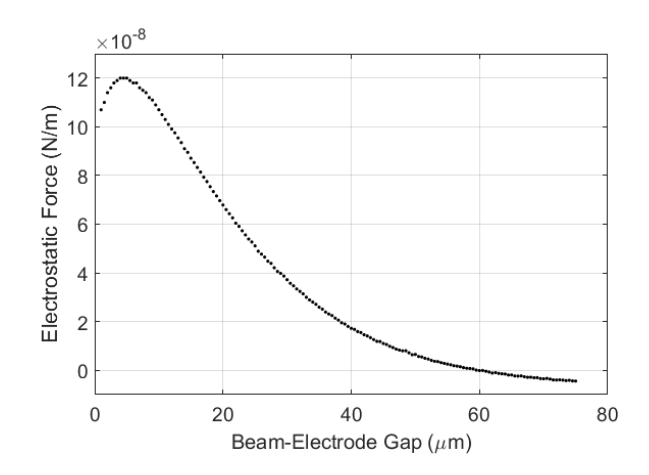


FIGURE 2. ELECTROSTATIC FORCE DATA FROM COMSOL

where \hat{w} is the z-direction beam displacement, I is the moment of inertia, V is the side electrode voltage, and \hat{f}_e is the electrostatic force at 1V. The electrostatic force profile is determined with a 2D COMSOL simulation. A 5th order polynomial is needed adequately fit the COMSOL data to be used with Equation (1). The electrostatic force profile can be seen in Fig. 2.

Equation (1) is non-dimensionalized using the substitutions shown in Tab. 2, which gives the non-dimensional equation of motion as,

$$\frac{\partial^2 w}{\partial t^2} + c^* \frac{\partial w}{\partial t} + \frac{\partial^4 w}{\partial x^4} + r_1 V^2 \sum_{j=0}^5 p_j h^j w^j = 0$$
 (2)

where p_j are constants from the 5th order polynomial forcing fit. Equation (2) is then reduced into a set of coupled ordinary

TABLE 1. BEAM GEOMETRY AND MATERIAL PROPERTIES

Parameter	Symbol	Value
Cantilever Length (µm)	L	500
Beam Width (μm)	b	17.5
Beam Height (µm)	h	2
Beam-Electrode Gap (µm)	g	2
Electrode Gap (µm)	g1	20.5
Electrode Width 1 (µm)	<i>b</i> 1	30
Electrode Width 2 (µm)	<i>b</i> 2	28
Electrode Thickness (µm)	h1	0.5
Elastic Modulus (GPa)	E	158
Density (kg/m^3)	ρ	2330
Poisson's Ratio	v	0.22
Force Constant	p_5	-8.5695×10^{14}
Force Constant	p_4	1.7347×10^{11}
Force Constant	p_3	-1.2595×10^{7}
Force Constant	p_2	3.5574×10^{2}
Force Constant	p_1	-3.8677×10^{-4}
Force Constant	p_0	-1.1703×10^{-7}

TABLE 2. NONDIMENSIONAL SUBSTITUTIONS

Parameter	Substitution
x-direction position	$x = \hat{x}/L$
z-direction position	$w = \hat{w}/h$
Time	$t = \hat{t}/T$
Damping	$c^* = \hat{c}L^4/EIT$
Time Constant	$T=\sqrt{ ho^{AL^4/EI}}$
Force Constant	$r_1 = L^4/EIh$

differential equations (ODE) through Galerkin's method. First, separation of variables is performed on Equation (2), with the

beam response approximated as,

$$w(x,t) \approx \sum_{i=1}^{n} q_i(t)\phi_i(x)$$
 (3)

where $\phi_i(x)$ are the mode shapes of the beam, $q_i(t)$ are the time dependent generalized coordinates, and n is the number of degrees of freedom (DOF). The effect of the electrostatic force on the mode shapes of the beam is neglected and thus the mode shapes for a cantilever micro-beam are given in Equation (4).

$$\phi_i(x) = \cosh(\alpha_i x) - \cos(\alpha_i x) - \sigma_i(\sinh(\alpha_i x) - \sin(\alpha_i x)) \quad (4)$$

where α_i are the square root of the non-dimensional natural frequencies, and σ_i are constants determined from the boundary conditions and mode to be considered. α_i and σ_i for the first three modes are obtained from [21].

Once the mode shapes are known, Equation (3) is plugged into the non-dimensional equation of motion (Equation (2)), which yields a coupled set of n ODE's for q_i .

$$\sum_{i=1}^{n} \left(\phi_i \frac{\partial^2 q_i}{\partial t^2} + c^* \phi_i \frac{\partial q_i}{\partial t} + \frac{\partial^4 \phi_i}{\partial x^4} q_i + r_1 V^2 \sum_{j=0}^{5} p_j h^j (q_i \phi_i)^j \right) = 0$$
(5)

To decouple the linear terms, Equation (5) is multiplied by ϕ_k and integrated over the length of the beam, resulting in,

$$m_i \ddot{q}_i + c_i \dot{q}_i + k_i q_i + r_1 V^2 \sum_{i=0}^{5} f_{ijk} q_i^j = 0$$
 (6)

where nonlinear terms remain coupled and,

$$m_{i} = \int_{0}^{1} \phi_{i}^{2} dx \quad k_{i} = \int_{0}^{1} \frac{d^{4} \phi_{i}}{dx^{4}} \phi_{i} dx \quad c_{i} = c^{*} m_{i}$$

$$f_{ijk} = p_{j} h^{j} \int_{0}^{1} \phi_{k} \phi_{i}^{j} dx$$
(7)

For a one mode approximation, Equation (6) becomes,

$$m_1\ddot{q}_1 + c_1\dot{q}_1 + k_1q_1 + r_1V^2 \sum_{i=0}^{5} f_i q_1^i = 0$$
 (8)

where

$$f_j = p_j h^j \int_0^1 \phi_1^{j+1} dx \tag{9}$$

A one mode model is used because one DOF is a very good approximation of the system, as verified in our previous experiment [12].

The last two terms that need to be defined are the damping constant, c, and the driving voltage V. The damping is estimated using the quality factor, Q and the relation shown below.

$$c = \frac{\alpha_1^2}{O} \tag{10}$$

The quality factor is assumed to be 100 to simulate a low damping environment. The driving voltage, V, is a sinusoidal AC voltage super imposed on a much larger DC voltage. The DC voltage will move the beam to some static position above the substrate, and the AC will cause the beam to vibrate about its static equilibrium point. A large DC voltage is required to give the beam enough room to vibrate without hitting the electrode. Once all terms are defined, Equation (8) can be solved.

Mathieu's Equation

To predict where parametric resonance (PR) will occur, Equation (8) can be related to the damped Mathieu's Equation, shown below.

$$\frac{d^2x}{d\tau^2} + c\frac{dx}{d\tau} + (\delta + \varepsilon\cos(\tau))x = 0$$
 (11)

Mathieu's Equation shows unbounded parametric resonance when $\delta = 1/4, 1, 9/4,...$ etc, and ε is large enough to overcome the beam damping c [22]. Equation (8) can be put in the form of Equation (11) to find at what driving frequency PR will occur.

First, the electrostatic force is linearized about the static equilibrium point, w = s (resulting from the DC component of the applied voltage), using a Taylor Series.

$$f_{e} \approx \beta_{1}q_{1} + \beta_{0} = \sum_{j=0}^{5} \left(p_{j}h^{j} \int_{0}^{1} \phi_{1}dx \right) s^{j} +$$

$$\sum_{j=1}^{5} \left(jp_{j}h^{j} \int_{0}^{1} \phi_{1}dx \right) s^{j-1} \left(\phi_{1}q_{1} - s \right)$$
(12)

Plugging the linearized force back into Equation (8) yields,

$$m_1 \ddot{q}_1 + c_1 \dot{q}_1 + k_1 q_1 + r_1 (V_{DC} + V_{AC} \cos(\omega t))^2 (\beta_1 q_1 + \beta_0) = 0$$
(13)

Using trigonometric identities, with $\tau = \omega t$, and combining linear terms yields the forced Mathieu's Equation with two time

scales.

$$\frac{dq_1^2}{d\tau^2} + 2\zeta \frac{\omega_n}{\omega} \frac{dq_1}{d\tau} + \left[\delta_1 + \varepsilon_{11}\cos(\tau) + \varepsilon_{21}\cos(2\tau)\right] q_1 = -\left(\frac{r_1\beta_0\tilde{V}_{DC}^2}{m\omega^2} + \varepsilon_{10}\cos(\tau) + \varepsilon_{20}\cos(2\tau)\right) \tag{14}$$

where

$$2\zeta \omega_{n} = \frac{c_{1}}{m_{1}} \quad \omega_{n} = \sqrt{\frac{k_{1}}{m_{1}}}$$

$$\delta_{1} = \frac{1}{\omega^{2}} \left(\omega_{n}^{2} + \frac{r_{1}\beta_{1}\tilde{V}_{DC}^{2}}{m} \right) \quad \varepsilon_{1i} = \frac{2r_{1}\beta_{i}V_{DC}V_{AC}}{m\omega^{2}} \qquad (15)$$

$$\varepsilon_{2i} = \frac{r_{1}\beta_{i}V_{AC}^{2}}{2m\omega^{2}} \quad \tilde{V}_{DC}^{2} = V_{DC}^{2} + \frac{V_{AC}^{2}}{2}$$

Equation (14) has both parametric resonance arising from the linear term, and normal resonance associated with the forcing terms. As mentioned above, there are also two time scales, τ and 2τ , for the ε_{1i} and ε_{2i} terms. Since the DC voltage is typically much larger than the AC voltage, the second term, ε_{2i} , will be much smaller than ε_{1i} . Because of this, our efforts are mainly focused on studying the resonance of the first time, though the effects of both are included in the analysis.

To find the frequency at which parametric resonance occurs, the δ_1 term is set equal to $\frac{1}{4}$ [22], and rearranged to find ω , the AC voltage frequency.

$$\omega = 2\sqrt{\left(\omega_n^2 + \frac{r_1\beta_1\tilde{V}_{DC}^2}{m}\right)} \tag{16}$$

where the square root term is the natural frequency with the stiffening effect of the applied voltage. Since β_1 is almost always positive, increasing DC voltage increases the natural frequency, which was verified in our previous experiment [12]. From Equation (16), one can see primary parametric resonance occurs at twice the natural frequency, as expected.

It is also important to note that since the original equation of motion (Equation (8)) has a quadratic non-linearity, the system will also show superharmonic and subharmonic resonances of order 2. This means that at twice the natural frequency, there will be both parametric and subharmonic resonance. These can be differentiated from each other by observing the time signal and phase portrait.

SIMULATION RESULTS

First, Equation (13) is solved using long time integration at approximately twice the natural frequency, which should show

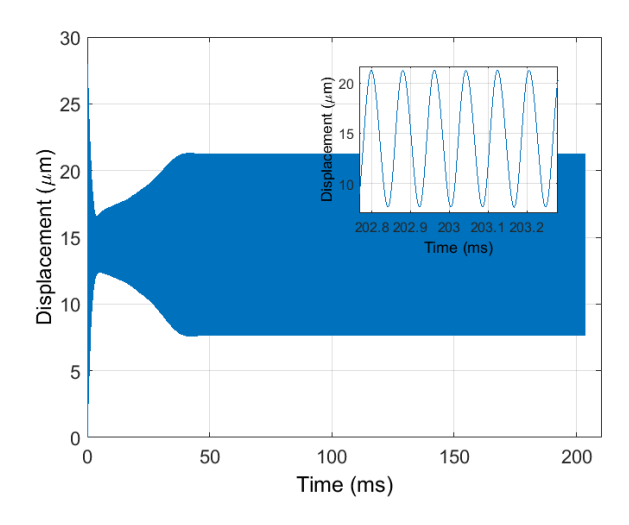


FIGURE 3. TIME RESPONSE AT 24.6 kHz WITH V_{DC} =187 V AND V_{AC} =7.5 V

parametric resonance (Equation (16)) if the excitation level is high enough. Fig. 3 shows a time response in this region. As can be seen in Fig. 3, the beam experiences parametric resonance at twice the natural frequency.

An indicator of parametric resonance can be seen in the steady state time response, which is shown in the inlet of Fig. 3. For parametric resonance, the time response period should be the same as the excitation period, while for subharmonic resonance the response period is twice the excitation period (period-2). Since both parametric and subharmonic resonance should occur, the period of the beam response can be an indicator as to which is dominant. This can be more clearly seen in the phase portrait of the steady state time response shown in Fig. 4.

The phase portrait shows the steady state response is parametric. Since the threshold for parametric resonance is usually higher than with subharmonic resonance, decreasing the AC voltage should show that the period doubles once the system has left the instability tongue for parametric resonance. Figure 5 shows the phase portrait when the AC voltage is decreased to 6.75 V. At 6.75 V_{AC} , the system shows subharmonic resonance. The oscillation amplitude is also much smaller than that of parametric resonance (Fig. 4), which shows the subharmonic contribution to the overall response is relatively small.

After the type of resonance was determined, a frequency sweep was conducted using the shooting method to capture both the stable and unstable steady-state trajectories. The shooting method is a computationally efficient numerical ODE solution method where initial conditions are guessed and continually updated to try and catch the steady-state response. A frequency response for several AC voltages can be seen in Fig. 6.

The system can achieve very large dynamic amplitudes

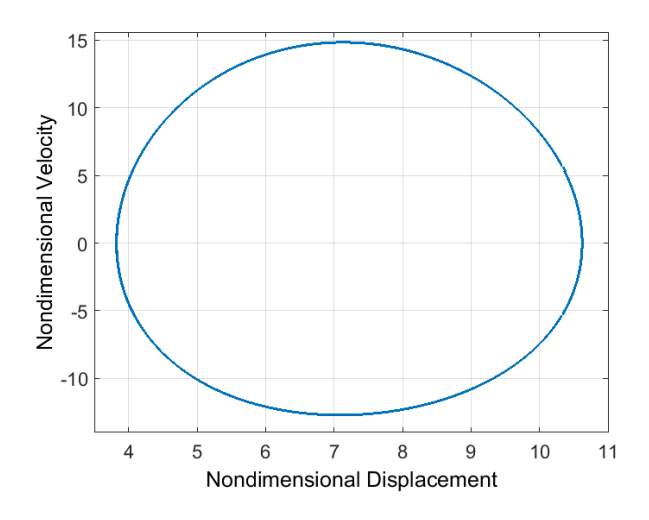


FIGURE 4. PHASE PORTRAIT OF THE STEADY STATE RESPONSE AT 24.6 kHz WITH V_{DC} =187 V AND V_{AC} =7.5 V

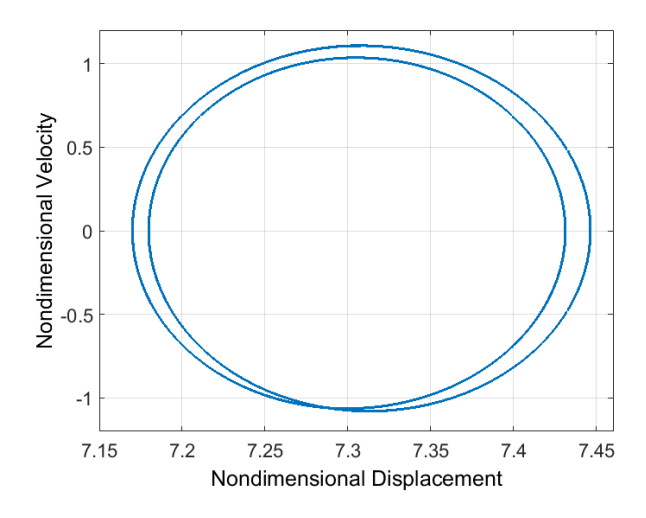


FIGURE 5. PHASE PORTRAIT OF THE STEADY STATE RESPONSE AT 24.6 kHz WITH V_{DC} =187 V AND V_{AC} =6.75 V

from parametric resonance (over $15\mu m$), however, an AC voltage of at least 30V is necessary to overcome the threshold voltage for parametric resonance when the DC voltage is 120V. This is high because the electrostatic force is generated through fringing electric fields, which are fairly weak. It is also important to note that on the backsweep branch the amplitude becomes large enough to collide with the electrode. Since the beam is only $2\mu m$ above the substrate, it can only reach approximately 2x the static deflection (for a total of $20\mu m$ in Fig. 6) before this becomes an issue. As seen in our previous experiment, as the beam gets close to the electrode squeeze film damping starts to occur, how-

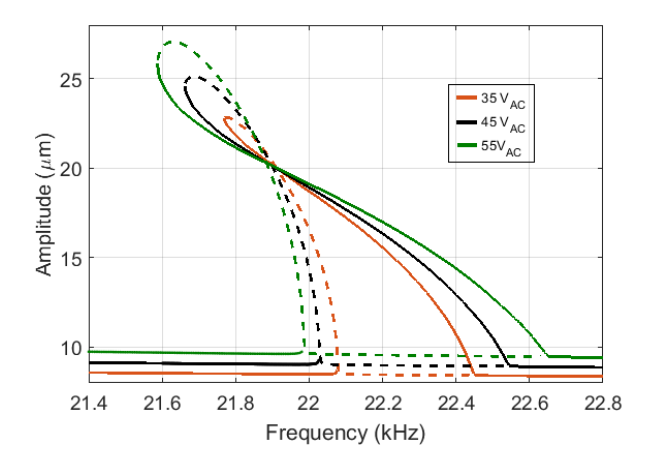


FIGURE 6. FREQUENCY RESPONSE AT $120V_{DC}$ AND 35, 45, and 55 V_{AC} . SOLID LINES INDICATE STABLE SOLUTIONS WHILE THE DASHED LINE INDICATES UNSTABLE SOLUTIONS.

ever this is not accounted for in our model.

Also shown in Figure 6, if the AC voltage is large enough, the unstable branch intersects with the stable branch. This creates a small bulge at the peak of the frequency curve that gets larger as the AC voltage is increased. This intersection disappears if the AC voltage is near the threshold for parametric resonance. At $120\ V_{DC}$ the threshold for parametric resonance is $30\ V_{AC}$, which is large.

The threshold voltage is dependent on the coefficient of the cosine term in Equation (14), ε_{11} . As can be seen in Equation (15), ε_{11} depends on both the AC and DC voltage. Because of this, increasing the DC voltage can lower the threshold AC voltage. Figure 7 shows a frequency sweep at 187 V_{DC} . When the DC voltage is increased up to 187 V, the threshold AC voltage drops significantly. As can be seen in Figure 7, 10 V_{AC} is enough to create a large parametric resonance with a larger amplitude and bandwidth than with 55 V_{AC} and 120 V_{DC} . The nonlinear behavior is also reduced because of the lower excitation level. In this case, the threshold AC voltage is reduced to about 7 V.

Since the shooting method is computationally fast and can predict unstable trajectories, it can also be used to map the parametric instability tongue. This is shown in Fig. 8 for the case of V_{DC} =187 V. In Fig. 8, the unstable region is where parametric resonance occurs. The instability tongue shows a minimum threshold voltage of about 7 V_{AC} when the quality factor is 100 (as mentioned above). This minimum threshold drops to 0 V when the damping from the system is removed. Figure 8 is also consistent with Fig. 4 and 5, showing the change from $7.5V_{AC}$ to $6.75V_{AC}$ crosses the instability threshold for 24.58kHz and results in only subharmonic resonance.

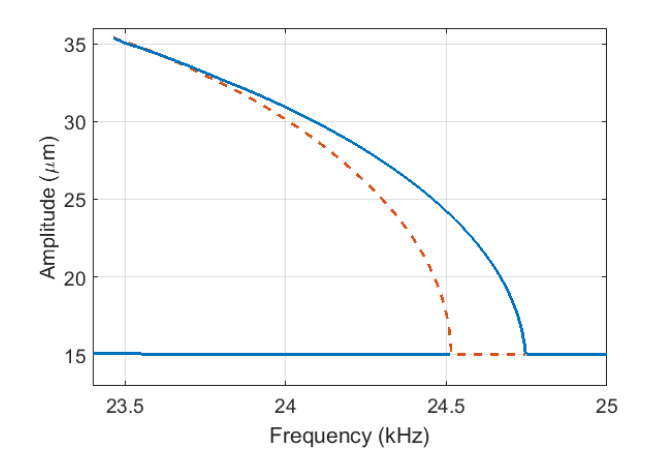


FIGURE 7. FREQUENCY RESPONSE AT $187V_{DC}$ AND $10V_{AC}$. SOLID BLUE LINES INDICATE STABLE SOLUTIONS WHILE THE DASHED ORANGE LINE INDICATES UNSTABLE SOLUTIONS.

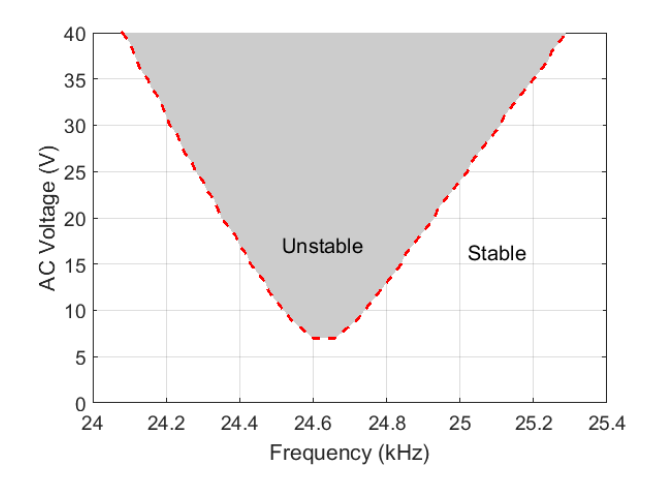


FIGURE 8. INSTABILITY TONGUE FOR PRIMARY PARAMETRIC RESONANCE AT $187V_{DC}$

CONCLUSION

In this paper, primary parametric resonance of a repulsive force fringe field resonator is reported. This results from the fringe field associated with the electrostatic force and occurs at twice the natural frequency of the system. Dynamic amplitudes as high as $20\mu m$ can be theoretically achieved at $187V_{DC}$ and $10V_{AC}$, however in application the beam would hit the middle electrode before this would occur.

Using Mathieu's Equation, the system was also shown to have both parametric and subharmonic resonance or order 2 at the same frequency. This is due to the nonlinearity of the elec-

trostatic force, however the effects of the subharmonic resonance is small as compared to the parametric component.

There was also found to be two time-scales associated with the parametric resonance, which arise from the superimposed AC and DC voltages. Since the DC voltage is much higher than the AC voltage, the faster term (ε_{11}) is much larger than the slower term (ε_{21}) . This means the primary parametric resonance is mainly dependent on the faster term.

REFERENCES

- [1] Younis, M. I., 2011. *MEMS Linear and Nonlinear Statics and Dynamics*. Springer, New York.
- [2] Lee, K. B., and Cho, Y. H., 2001. "Laterally driven electrostatic repulsive-force microactuators using asymmetric field distribution". *Journal of Microelectromechanical Systems*, 10(1), pp. 128–136.
- [3] Sugimoto, T., Nonaka, K., and Horenstein, M. N., 2005. "Bidirectional electrostatic actuator operated with charge control". *Journal of Microelectromechanical Systems*, 14(4), pp. 718–724.
- [4] Shen, N., and Kan, E., 2002. "Novel electrostatic repulsion forces in MEMS applications by nonvolatile charge injection". Technical Digest. MEMS 2002 IEEE International Conference. Fifteenth IEEE International Conference on Micro Electro Mechanical Systems (Cat. No.02CH37266), pp. 598–601.
- [5] He, S., and Mrad, R. B., 2005. "Large-stroke microelectrostatic actuators for vertical translation of micromirrors used in adaptive optics". *IEEE Transactions on Industrial Electronics*, *52*(4), pp. 974–983.
- [6] He, S., and Mrad, R. B., 2008. "Design, modeling, and demonstration of a MEMS repulsive-force out-of-plane electrostatic micro actuator". *Journal of Microelectrome-chanical Systems*, 17(3), pp. 532–547.
- [7] He, S., and Mrad, R. B., 2009. "Development of a multi-level repulsive force out-of-plane micro electrostatic actuator". *IECON Proceedings (Industrial Electronics Conference)*, pp. 4020–4023.
- [8] Chong, J., He, S., and Mrad, R. B., 2010. "Control of a surface micromachined repulsive-force driven 2D micromirror". IEEE/ASME International Conference on Advanced Intelligent Mechatronics, AIM, pp. 1005–1007.
- [9] Fan, C., and He, S., 2015. "A Two-Row Interdigitating-Finger Repulsive-Torque Electrostatic Actuator and Its Application to Micromirror Vector Display". *Journal of Microelectromechanical Systems*, 24(6), pp. 2049–2061.
- [10] Li, G., Guo, X., Zhao, Q., and Hu, J., 2015. "An Electrostatic Repulsive-Force Based Micro Actuator for Capacitive RF MEMS Switch". pp. 1095–1098.
- [11] Qiao, D. Y., Yuan, W. Z., and Li, X. Y., 2006. "Design of an electrostatic repulsive-force based vertical micro actua-

- tor". Proceedings of 1st IEEE International Conference on Nano Micro Engineered and Molecular Systems, 1st IEEE-NEMS(90407020), pp. 168–171.
- [12] Pallay, M., Daeichin, M., and Towfighian, S., 2016. "Dynamic Behavior of an Electrostatic MEMS Resonator with Repulsive Actuation". *Nonlinear Dynamics*. doi:10.1007/s11071-017-3532-z.
- [13] Rugar, D., and Grütter, P., 1991. "Mechanical parametric amplification and thermomechanical noise squeezing". *Physical Review Letters*, **67**(6), pp. 699–702.
- [14] Zhang, W.-M., and Meng, G., 2007. "Nonlinear dynamic analysis of electrostatically actuated resonant MEMS sensors under parametric excitation". *IEEE Sensors Journal*, 7(3), pp. 370–380.
- [15] Harish, K. M., Gallacher, B. J., Burdess, J. S., and Neasham, J. a., 2008. "Experimental investigation of parametric and externally forced motion in resonant MEMS sensors". *Journal of Micromechanics and Microengineer*ing, 19(1), p. 015021.
- [16] Hu, Z., Gallacher, B. J., Harish, K. M., and Burdess, J. S., 2010. "An experimental study of high gain parametric amplification in MEMS". *Sensors and Actuators, A: Physical*, *162*(2), pp. 145–154.
- [17] Sharma, M., Sarraf, E. H., and Cretu, E., 2013. "Shaped combs and parametric amplification in inertial MEMS sensors". *IEEE SENSORS 2013 Proceedings*, 1(1), pp. 1–4.
- [18] Jia, Y., Yan, J., Soga, K., and Seshia, A. a., 2013. "Parametrically excited MEMS vibration energy harvesters with design approaches to overcome the initiation threshold amplitude". *Journal of Micromechanics and Microengineering*, 23(11), p. 114007.
- [19] Krylov, S., Harari, I., and Cohen, Y., 2005. "Stabilization of electrostatically actuated microstructures using parametric excitation". *Journal of Micromechanics and Microengineering*, 15(6), pp. 1188–1204.
- [20] Linzon, Y., Ilic, B., Lulinsky, S., and Krylov, S., 2013. "Efficient parametric excitation of silicon-on-insulator microcantilever beams by fringing electrostatic fields". *Journal of Applied Physics*, *113*(16).
- [21] Rao, S. S., 2010. Mechanical Vibrations, Vol. 67.
- [22] Rand, R. H., and Rand, R., 2005. "Lecture Notes on Nonlinear Vibrations". *Coexistence*.